References

[1] C.T Seaton, J.D. Valera, R.L. Shoemaker, G.I. Stegeman, J.T. Chilwell, S.D. Smith, 'Calculations of nonlinear TE waves guided by thin dielectric film bounded by nonlinear media', *IEEE, Journal of Quantum Electronics*, vol.21, 1985, pp. 774-783.

[2] B.M.A. Rahman, J.B. Davies, 'Finite element solution of nonlinear bistable optical waveguides', *International Journal of Optoelectronics*,vol. 4, 1989, pp. 153-161.

[3] R.A. Sammut, Q.Y. Li, C. Pask, 'Variational approximations and mode stability in planar nonlinear waveguides', *Journal of Optical Society of America B*, vol.9, 1992, pp. 884-890.

[4] A.B. Aceves, P. Varatharajah, A.C. Newell, E.M. Wright, G.I. Stegeman, D.R. Heatley, J.V. Moloney, H. Adachihara, 'Particle aspects of collimated light channel propagation at nonlinear interface and in waveguides', *Journal of Optical Society of America B*, vol.7, 1990, pp. 963-974.

[5] A.D. Boardman, T. Twardowski, 'Theory of nonlinear interaction between TE and TM waves', *Journal of Optical Society of America B*, vol.5, 1988, pp. 523-528.

[6] S. Vukovic, R. Dragila, 'Power - flux - dependent polarization of nonlinear surface Waves', *Optics Letters*, vol.15, 1990, pp. 168-170.

[7] K. Hayata, A. Misawa, M. Koshiba, 'Nonstationary simulation of nonlinearly coupled TE-TM waves propagating down dielectric slab structures by the step-by-step finite-element method', *Optics Letters*, vol.15, 1990, pp. 24-26.

[8] M. Zoboli, S. Selleri, 'Finite element analysis of TE and TM modes in nonlinear planar waveguides', to be published in *International Journal of Nonlinear Optical Physics*, vol.3, 1994.

[9] M.Zoboli, F. Di Pasquale, S.Selleri, 'Full vectorial and scalar solutions of nonlinear optical fibers', *Optics Communications*, vol.97, 1993, pp. 11-15.

[10] M.Zoboli, P.Bassi, *The finite element method for anisotropic optical waveguides*, from "Anisotropic and Nonlinear Optical Waveguides", edited by G.Stegeman and C.G.Someda, ELSEVIER 1992, pp. 77-116.

[11] K. Hayata, A. Misawa, M. Koshiba, 'Spatial polarisation instabilities due to transverse effects in nonlinear guided-wave system', *Journal of Optical Society of America B*, vol.7, 1990, pp.1268-1280.

[12] P.D. Maker, R.W. Terhune, C.M. Savage, 'Intensity dependent changes in the refractive index of liquids', *Physical Review Letters*, vol.12, 1964, pp.507-509.

COMPEL – The International Journal for Computation and Mathematics in Electrical and Electronic Engineering
Vol. 13, Supplement A, 353–358 © 1994 James & James Science Publishers Ltd

Modal Spectrum Of The Ridged Circular Waveguide Using The FE Method

A. Alvarez Melcon, R. Molina and M. Guglielmi
European Space Research and Technology Center. P.O. Box 299
Noordwijk, The Netherlands. Fax: 31-1719-84596. Tel: 31-1719-83193

Abstract

In this paper, results on the modal spectrum analysis of a Ridged Circular Waveguide (RCW) obtained with the Finite Element Method (FEM) are presented. The results obtained show that the RCW can be used in dual mode filters to eliminate the Tuning Screws unit traditionally required for this kind of hardware.

First a brief theoretical discussion is presented with explanation of the mathematic algorithms used to solve the problem, then some of the results obtained are presented including the scalar potential distributions and the eigenvalues for both TE and TM modes in the RCW as obtained with the FEM analysis. The problems encountered are also discussed and finally an assessment of the numerical technique used is presented.

Numerical Implementation

The problem of the modal spectrum analysis of a uniform section of RCW as shown in fig. 1 has been accomplished by the use of the FEM technique. This problem is very important since its solution can lead to CAD packages for the rigorous analysis of dual mode filters (fig. 2).

In this study a solution to the Helmholtz equation is sought for both TE and TM boundary conditions [1], namely:

$$\vec{\nabla}_t^{\,2}\phi + k_t^2\phi = 0 \tag{1}$$

in the domain defined by the RWC. This equation is known as the strong formulation of the problem and involves second order derivatives of the unknown scalar potential ϕ. Multiplying (1) by a suitable weighting function w and integrating over the whole RCW cross section Ω we obtain the following expression:

$$\int_\Omega w \cdot \nabla^2\phi \cdot d\Omega + \int_\Omega w \cdot k_t^2 \cdot \phi \cdot d\Omega = 0 \tag{2}$$

By applying Green's identity to equation (2) we can obtain the following expression known as the weak formulation of the problem, since it involves only first derivatives of the unknown function.

$$\int_\Gamma w \cdot \vec{\nabla}_t\phi \cdot \vec{n} \cdot d\Gamma - \int_\Omega \vec{\nabla}_t w \cdot \vec{\nabla}_t\phi \cdot d\Omega + k_t^2 \int_\Omega w \cdot \phi \cdot d\Omega = 0 \tag{3}$$

In equation (3), Ω is the domain where a solution to the problem is sought (the RCW cross section), Γ is its boundary and w is a suitable weighting function. Equation (3) can now be discretized using a first order finite element method. The discretization of the RCW cross section

was accomplished by using triangular elements. The integrals in eq (3) can now be evaluated in each element, and the final value of the integrals are computed by summing the values for all the elements in the discretization, that is:

$$\sum_e \int_{\Gamma_e} w \cdot \vec{\nabla}_t \phi \cdot \vec{n} \cdot d\Gamma_e - \sum_e \int_{\Omega_e} \vec{\nabla}_t w \cdot \vec{\nabla}_t \phi \cdot d\Omega_e + k_t^2 \sum_e \int_{\Omega_e} w \cdot \phi \cdot d\Omega_e = 0 \tag{4}$$

In equation (4) Ω_e is an element in the discretization of the RCW cross section, and Γ_e is the side of the boundary of an element at the border of the waveguide.

The nature of the solution obtained in (4) depends on the type of boundary conditions imposed. For TE modes we have that in a metallic wall

$$\frac{\partial \phi}{\partial n} = \vec{\nabla}_t \phi \cdot \vec{n} = 0 \tag{5}$$

and therefore the first integral of equation (4) becomes zero. For TM modes instead, the scalar potential must be zero in the border of the waveguide, that is $\phi = 0$. This condition will force the weighting function to be zero in the border and therefore the first integral in (4) will also be zero. The discretized basic equation then becomes for both TE and TM modes

$$k_t^2 \sum_e \int_{\Omega_e} w \cdot \phi \cdot d\Omega_e = \sum_e \int_{\Omega_e} \vec{\nabla}_t w \cdot \vec{\nabla}_t \phi \cdot d\Omega_e \tag{6}$$

which forms the basic system of linear equations to be solved for the unknown ϕ. The first integral to be solved in a generic element e of the mesh is:

$$I_1^{(e)} = \int_{\Omega_e} w \cdot \phi \cdot d\Omega_e \tag{7}$$

To solve this integral we first expand the unknown scalar potential in terms of a set of suitable shape functions, namely

$$\phi(x, y) = \sum_{i=1}^{3} \phi_i \cdot N_i(x, y) \tag{8}$$

where ϕ_i are the values of the scalar potential in the three nodes of the triangular element e and N_i is the shape function of the element e related to node i. The integral in equation (7) will be computed through the following average operation

$$I_1^{(e)} = \bar{w} \cdot \bar{\phi} \cdot A_e \tag{9}$$

where $\bar{w}$ is the average value of the weighting function in the current element, $\bar{\phi}$ is the average value of the scalar potential in the current element, and A_e is the area of the current element. If we take the weighting function the same as the shape function we can finally write:

$$I_1^{(e)} = \frac{1}{3} \cdot \frac{1}{3} \cdot A_e \cdot \sum_{i=1}^{3} \phi_i \tag{10}$$

The last step in the formulation of the problem is the computation of the second integral in equation (4) and in a generic element e of the mesh, namely:

$$I_2^{(e)} = \int_{\Omega_e} \vec{\nabla}_t w \cdot \vec{\nabla}_t \phi \cdot d\Omega_e \tag{11}$$

Taking again as a weighting function the same shape function, what is left is the computation of

$$\int_{\Omega_e} \vec{\nabla}_t N_i \cdot \vec{\nabla}_t \phi \cdot d\Omega_e = \int_{\Omega_e} \left(\frac{\partial N_i}{\partial x} \cdot \frac{\partial \phi}{\partial x} + \frac{\partial N_i}{\partial y} \cdot \frac{\partial \phi}{\partial y} \right) \tag{12}$$

using the expansion defined in (8) and taking derivatives, we can write

$$\vec{\nabla}_t \phi(x, y) = \sum_{i=1}^{3} \phi_i \cdot \vec{\nabla}_t N_i(x, y) \tag{13}$$

therefore it is straight forward that

$$\frac{\partial \phi}{\partial x} = \sum_{i=1}^{3} \phi_i \cdot \frac{\partial N_i}{\partial x} \tag{14}$$

$$\frac{\partial \phi}{\partial y} = \sum_{i=1}^{3} \phi_i \cdot \frac{\partial N_i}{\partial y} \tag{15}$$

so that the only thing which is left is the evaluation of the shape functions derivatives. They will be computed by first averaging them on the element level that is:

$$\frac{\partial \bar{N}_i}{\partial x} = \frac{1}{A_e} \cdot \int_{\Omega_e} \frac{\partial N_i}{\partial x} \cdot d\Omega_e \tag{16}$$

$$\frac{\partial \bar{N}_i}{\partial y} = \frac{1}{A_e} \cdot \int_{\Omega_e} \frac{\partial N_i}{\partial y} \cdot d\Omega_e \tag{17}$$

and then applying Green's identity to finally obtain

$$\frac{\partial \bar{N}_i}{\partial x} = \frac{1}{A_e} \cdot \int_{\Gamma_e} N_i \cdot n_x \cdot d\Gamma_e \tag{18}$$

$$\frac{\partial \bar{N}_i}{\partial y} = \frac{1}{A_e} \cdot \int_{\Gamma_e} N_i \cdot n_y \cdot d\Gamma_e \tag{19}$$

where n_x and n_y are the x and y components of the vector normal to the element e in the discretization. Using these expressions for the integrals, the system in (6) can be written in the following matrix form:

$$K \cdot \vec{\phi}^{(j)} = M \cdot \vec{\phi}^{(j-1)} \tag{20}$$

where the matrices K and M are built from the discretization of the integrals $I_1^{(e)}$ and $I_2^{(e)}$. This last equation can be solved by using the inverse iteration algorithm [2]. In eq. (20) $\vec{\phi}^{(j)}$ is a vector containing the values of the scalar potential in all the nodes of the mesh for the j_{th} iteration and $\vec{\phi}^{(j-1)}$ is the corresponding vector in the previous iteration. The inverse iteration procedure is used with a subsequent Gram-Schmidt orthogonalization to force the solution to be orthogonal with all previous solutions [2], thus obtaining a set of orthogonal scalar mode functions. The solution is now completed by computing the eigenvalue through the following normalization operation

$$k_t^{(j)^2} = \frac{\|\vec{\phi}^{(j)}\|}{\vec{\phi}^{(j)}} \tag{21}$$

So after a number of iterations j, the vector $\vec{\phi}^{(j)}$ is expected to converge to the scalar potential distribution of the current TE or TM mode along the RCW cross section, and $k_t^{(j)}$ to its eigenvalue. For the efficient implementation of this numerical method, the system of linear equations represented by (20) was solved using a conjugate gradient algorithm, which eliminates the problems of storage and is able to speed up considerably the global software.

Results

We present here the results of the analysis of the RCW obtained with the finite element technique. In fig. 3 and fig. 4 the scalar potential distribution for a TE and TM mode can be seen in a RCW (structure shown in fig. 1a). Furthermore, in Table I the eigenvalues of eight TE and TM modes for the RCW indicated are presented as obtained with the finite element analysis.

Table II shows the effect of a change in penetration of one pair of tuning ridges in the eigenvalues of the first TE degenerate modes. Finally in Table III we present the variation of the eigenvalues for the dominant degenerate modes when the penetration of the fifth ridge is varied (structure shown in fig. 1b).

During the realization of the previous analysis it was noticed that a large number of elements in the mesh was needed to get good accuracy, specially when the order of the mode was high. A total of fifty TE and TM modes were obtained using this method, but some of them could not be obtained with high accuracy. It was also observed that for some modes the convergency of the inverse iteration method was very slow resulting in a rotation of the scalar potential with respect the vertical and horizontal axis. Both negative effects are probably due to the presence of the corners in the RCW cross section; these corners are known to be problematic for the modelization using Finite Elements Techniques [3]. In the present analysis this was solved by taking a very fine mesh with a lot of elements (around 30.000 triangular elements with approximately 20.000 nodes were used), but this solution reduces the efficiency of the software, increasing the computational time. Alternatively one can try to use an adaptive meshing procedure to increase the refinement of the mesh nearby the corners while maintaining to a reasonable value the total number of elements in the discretization of the whole cross section.

Conclusions

A modal spectrum analysis of a RCW has been accomplished using the FEM approach. The results presented have demonstrated that the FEM technique can indeed be used for the analysis of the Ridged Circular Waveguide (RCW).

Some problems of accuracy and convergency were encountered. These problems can be partially solved by taking a very fine mesh in the discretization, but this solution increase the computational time of the software. As a consequence, when the complete dual-mode cavity is analyzed, the FEM portion of the code becomes inevitably the most time consuming part. The CPU time required for the FEM computations therefore is the main obstacle for the development of an efficient code for this particular application.

The efficiency of the algorithm can probably be increased by using an adaptive meshing procedure to represent with high accuracy the corners while maintaining in a relatively small value the total number of elements in the mesh. Further development work is in progress both with the FEM and other numerical approaches.

References

[1] N. Marcuvitz, *Waveguide Handbook*. New York: McGraw-Hill, 1951.

[2] J.F. Imbert, *Analyse des Structures par Elements Finis*. CEPADUES, Toulouse 1984.

[3] Fook Loy NG, *Tabulation of Methods for the Numerical Solution of the Hollow Waveguide Problem*. IEEE Transactions on Microwave Theory and Techniques, March 1974, pag. 322-328.

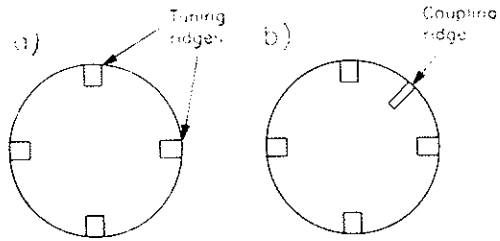

Fig. 1 Cross section of ridged circular waveguide. (a) Without coupling ridge. (b) With coupling ridge. 1.

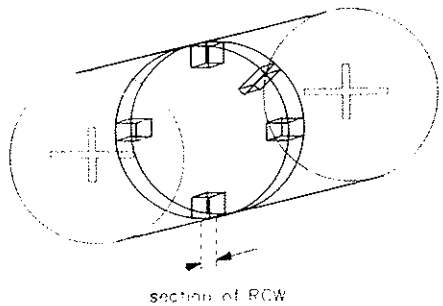

Fig. 2 Dual mode cavity using a section of ridged circular waveguide.

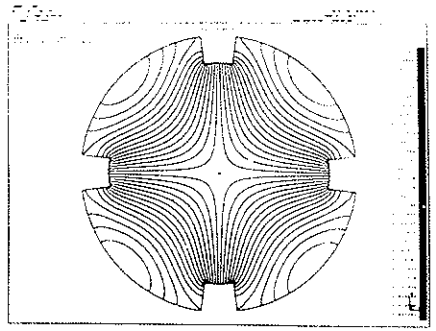

Fig. 3 Scalar potential distribution for a TE mode in the structure of fig. 1a, as obtained with the finite element method.

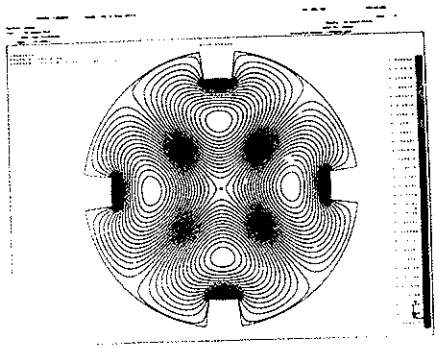

Fig. 4 Scalar potential distribution for a TM mode in the structure of fig. 1a, as obtained with the finite element method.

	TE	TM
n=1	1.8279	2.6435
n=2	1.8279	4.1631
n=3	2.6679	4.1631
n=4	3.3577	5.2129
n=5	3.8720	5.8722
n=6	4.0032	5.9444
n=7	4.0032	6.7116
n=8	4.5129	6.7116

Tab. I Eigenvalues for the first eight TE and TM modes of the ridged circular waveguide as in fig. 1a. All data were obtained through a finite element analysis. The four ridges in fig. 1a are 15° wide and $0.2a$ deep (a is the radius of the ridged circular waveguide).

	d/a = -0.1 (%)	d/a = -0.05 (%)	d/a = 0.00 (%)	d/a = 0.05 (%)	d/a = 0.1 (%)
n = 1	3.2075	1.4701	0.0000	-1.3030	-2.2720
n = 2	-6.1143	-3.5082	0.0000	4.5439	10.2573

Tab. II Percentage Variation of the eigenvalues of the lowest degenerate TE modes for the ridged circular waveguide in fig. 1a, as a function of the penetration of one pair of tuning ridges. Depth of one pair of ridges is kept the same as in Table I. The depth of the others is varied. d/a is the normalized variation.

	c/a = 0.05 (%)	c/a = 0.10 (%)	c/a = 0.15 (%)	c/a = 0.20 (%)	c/a = 0.25 (%)
n = 1	0.0167	0.2673	1.0023	1.9044	3.1741
n = 2	-0.2673	-0.5348	-1.1894	-1.5035	-1.8378

Tab. III Percentage variation of the transverse eigenvalues of the lowest degenerate TE modes for the ridged circular waveguide in fig. 1b when the penetration of the coupling ridge is varied (c/a is the relative penetration of the coupling ridge). The tuning ridges are kept as in Table I whereas the coupling ridge is 5° wide.

COMPEL – The International Journal for Computation and Mathematics in Electrical and Electronic Engineering
Vol. 13, Supplement A, 359–364 © 1994 James & James Science Publishers Ltd

Progress on the Application of the Finite Element Method for 3D Electromagnetic Scattering and Radiation

J. L. Volakis, A. Chatterjee, J. Gong, L. C. Kempel and D. C. Ross
Radiation Laboratory, Department of Electrical Engineering and Computer Science
The University of Michigan, Ann Arbor, MI 48109-2122

Abstract. Example calculations are presented using three different hybrid finite element formulations. Each of the hybrid finite element methods is best suited for a different class of problems.

Formulation

In this section we state the basic equations which lead to the various hybrid finite element formulations. Consider the geometry in Figure 1. The computational domain, V_0, is enclosed by an artificial surface S_0 and may contain scattering objects such as homogeneous dielectrics (V_d), metallic bodies (S_2) and resistive/impedance sheets (S_K). The appropriate weak-form of the wave equation satisfied by the total fields within V_0 is [1]

$$\iiint_{V_0}\left[\frac{1}{\mu_r}\nabla\times\mathbf{E}\cdot\nabla\times\mathbf{T}-k_0^2\epsilon_r\mathbf{E}\cdot\mathbf{T}\right]dv + jk_0Z_0\iint_{S_K}\frac{(\hat{n}\times\mathbf{E})\cdot(\hat{n}\times\mathbf{T})}{K}ds - jk_0Z_0\iint_{S_0}\hat{n}\times\mathbf{H}\cdot\mathbf{T}\,ds=0 \tag{1}$$

where $\mathbf{T}$ denotes the weighting function and S_K encompasses all resistive or impedance surfaces enclosed by S_0. The parameter K is equal to the normalized sheet resistivity or the normalized impedance. If S_0 enclosed a plate of varying impedance, then S_K must be replaced by the sum of the upper and lower plate surfaces.

For open-body scattering, it is desirable to work with the scattered fields ($\mathbf{E}^{\text{scat}}=\mathbf{E}-\mathbf{E}^{\text{inc}}$, $\mathbf{H}^{\text{scat}}=\mathbf{H}-\mathbf{H}^{\text{inc}}$), where ($\mathbf{E}^{\text{inc}},\mathbf{H}^{\text{inc}}$) denote the excitation fields. The appropriate weak form of the wave equation is then given by [2]

$$\begin{aligned}&\iiint_{V_0}\left[\frac{1}{\mu_r}\nabla\times\mathbf{E}^{\text{scat}}\cdot\nabla\times\mathbf{T}-k_0^2\epsilon_r\mathbf{E}^{\text{scat}}\cdot\mathbf{T}\right]dv\\&+jk_0Z_0\left[\iint_{S_K}\frac{\hat{n}\times\mathbf{E}^{\text{scat}}\cdot\hat{n}\times\mathbf{T}}{K}ds+\iint_{S_K}\frac{\hat{n}\times\mathbf{E}^{\text{inc}}\cdot\hat{n}\times\mathbf{T}}{K}ds\right]\\&-jk_0Z_0\iint_{S_0}\hat{n}\times\mathbf{H}^{\text{scat}}\cdot\mathbf{T}\,ds+\iiint_{V_d}\left[\frac{1}{\mu_r}\nabla\times\mathbf{E}^{\text{inc}}\cdot\nabla\times\mathbf{T}-k_0^2\epsilon_r\mathbf{E}^{\text{inc}}\cdot\mathbf{T}\right]dv\\&+jk_0Z_0\iint_{S_d}\frac{1}{\mu_r}\left(\hat{n}\times\mathbf{H}^{\text{inc}}\right)\cdot\mathbf{W}\,ds=0\end{aligned} \tag{2}$$

in which S_d is the aggregate of the surfaces enclosing the dielectrics occupying the volume V_d.